Dissipation Measurement with a Moored Instrument in a Swift Tidal Channel

ROLF LUECK AND DANIEL HUANG

School of Earth and Ocean Sciences, University of Victoria, Victoria, British Columbia, Canada

(Manuscript received 13 June 1997, in final form 28 October 1998)

ABSTRACT

A moored and autonomous instrument that measures velocity and temperature fluctuations in the inertial subrange using shear probes and FP07 thermistors has been deployed in a swift [$O(1\ m\ s^{-1})$] tidal channel for eight days. The measured velocity signals are free from body vibrations for frequencies below 16 Hz in flows faster than 0.5 m s^{-1} and below 8 Hz for slower flows. At lower frequencies, fluctuations of torque on the instrument, due mainly to fluctuations of the ambient current, produce large pitching and rolling motions ($\approx 4°$ peak) that can easily be reduced by minor mechanical changes. Vibrations at higher frequencies do not scale with flow speed and stem mainly from mechanical structures. The velocity spectrum is free from contamination by body motions between 0.2 and 20 cpm (the inertial subrange), and consistent estimates of the rate of dissipation of kinetic energy are obtained from the spectral levels of vertical and lateral velocity fluctuations within this range.

1. Introduction

The demand for time series of ever-increasing length and the escalating cost of ship and personnel time motivate the need for autonomous and automated measurement systems. The measurement of ocean turbulence and mixing is one of the least automated disciplines in physical oceanography and usually involves a team of workers and dedicated ship operations. The Tethered Autonomous Moored Instrument (TAMI) is designed to address this need for lengthy and unattended measurements of velocity and temperature microstructure, while providing data of the ''fine structure'' of temperature, salinity, and current and their vertical gradients.

TAMI was originally intended for use in the deep ocean and weak currents of $O(0.3\ m\ s^{-1})$. So far, it has been deployed only in coastal channels. This instrument was shown to function well in a sluggish coastal channel with currents of up to 0.15 m s^{-1} (Lueck et al. 1997, hereafter L97). Here, we build on L97 to demonstrate that this instrument can also function in very turbulent environments with flows of up to 1.2 m s^{-1}. The rate of dissipation of kinetic energy is estimated with the inertial subrange technique because the sampling rate is too slow and the Kolmogorov wavenumber is too high to permit the resolution of the dissipation range of velocity fluctuations.

This paper provides a brief description of TAMI (section 2), an example of velocity and motion time series (section 3), sample spectra (section 4), and a discussion of problems and potential solutions for this instrument (section 5).

2. Instrument

a. Mechanical features

A detailed description of the instrument TAMI is provided by L97. Only the features pertinent to this work are presented here. The main body of the instrument is a wing tank, 4.5 m long and 0.6 m in diameter at midbody (Fig. 1). A sailboat mast, 3.5 m long, is mounted vertically through the center of the body. A ball-bearing and oil-filled swivel, on the line attached to the bottom of the mast, permits the instrument to rotate in response to changes in the direction of the ambient current. Two vertical fins at the rear provide the torque for rotation, and two horizontal fins stabilize pitching motions. The rear of the horizontal stabilizers are bent downward for reasons discussed later. In ascending order, the mooring components consisted of a 300-kg cement anchor, a 1-m chain, an interocean acoustic release, a rubber-coated steel cable with a 10-m length and 0.008-m diameter, a swivel, and another 1-m segment of rubber-coated cable attached to the bottom of the mast. The swivel has the shape of a cylinder and is 0.12 m long and 0.05 m in diameter.

Pairs of Seabird temperature and conductivity sensors

Corresponding author address: Rolf Lueck, School of Earth and Ocean Sciences, University of Victoria, P.O. Box 1700, Victoria, BC V8W 2Y2, Canada.
E-mail: rlueck@uvic.ca

© 1999 American Meteorological Society

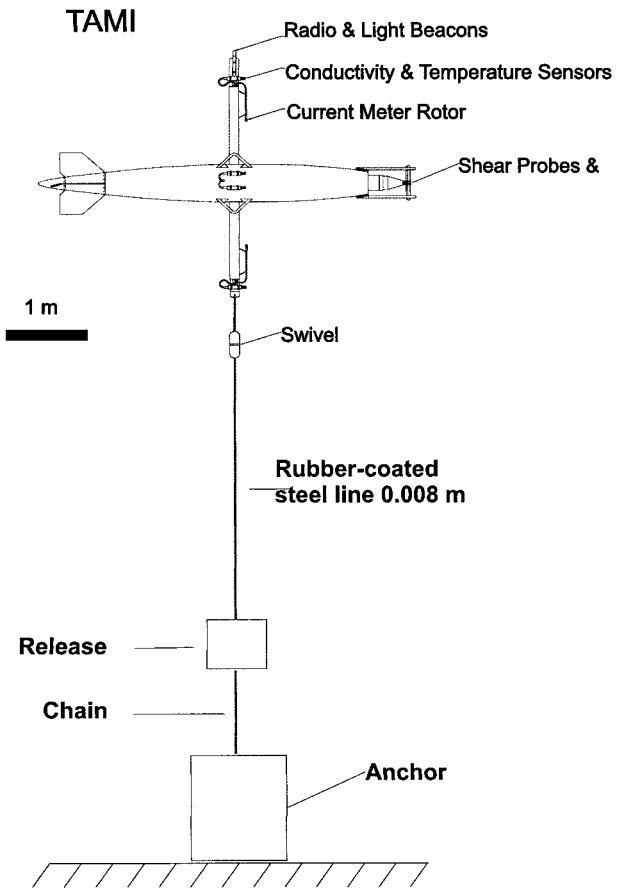

FIG. 1. Sketch of TAMI and the mooring arrangement used in Cordova Channel. The rubber-coated line is 10 m long and not drawn to scale. The instrument is at 15 mab during slack tide.

are mounted at the top and bottom of the mast, while a third pair is attached to the main body in line with the mast. The sensors at the top (bottom) of the mast are 1.5 m above (below) the sensors at midbody. The speed of the ambient current is measured by two rotor current meters (McPhee 1992) attached to the upper and lower half of the mast. The electronics are housed in a pressure case mounted in the forward half of the vehicle. The front end cap is conical and holds four shear probes and two FP07 thermistors on its exterior, and three orthogonal accelerometers and a flux-gate compass in its interior. A pressure transducer is attached to the rear end cap of this pressure case. A second pressure case containing batteries is mounted in the aft half of the body. A guard ring with a teardrop cross section is attached to the front of the body to protect the turbulence sensors without restricting the flow past these sensors.

The instrument weighs 4500 N in air and has a net buoyancy of 550 N, which is provided by a combination of fiberglass balls and syntactic foam. Buoyancy and weight can be attached inside the tail section for trimming the pitch of the body. The floodable volume is 0.12 m^3 and the total enclosed mass is 570 kg.

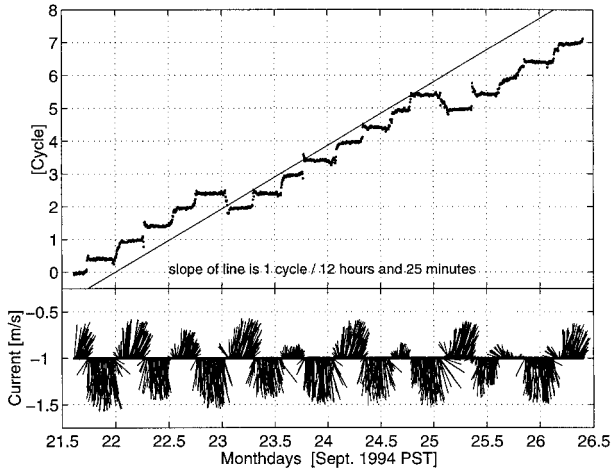

FIG. 2. Time series of current vectors (lower panel) rotated so that along-channel (northwesterly) flow is directed up. The instrument heading (upper panel) expressed in terms of whole rotations. The line fitted to the points is the phase of the lunar semidiurnal tide.

b. Electronics

Every 5 min, the instrument collects and processes 128 s of data. The shear probes, thermistors, and accelerometers are sampled 128 times per second, while the other sensors are sampled at slower rates. The rapidly sampled signals are processed into spectra from four periodograms of 32 s of data. These spectra are band averaged into 21 intervals of geometrically increasing width centered on 0.0315 to 56.0 Hz. Both the rapidly and lowly sampled data are processed into the statistics of mean, standard deviation, maximum, and minimum. The processed data are stored in nonvolatile memory and transferred to disk every 6 h. One unprocessed dataset is also recorded every 6 h. The sampling rate of 128 Hz and the low-pass filtering (43 Hz) are designed for currents of less than 0.3 m s^{-1} and do not provide sufficient bandwidth to resolve the shear spectrum for the typical currents of order 1 m s^{-1} found in Cordova Channel. However, the sampling rate does resolve the inertial subrange (section 4).

c. Deployment

The instrument was deployed twice in Cordova Channel from 1533 PST 21 September 1994 to 1046 PST 26 September 1994 and from 1146 PST 27 September 1994 to 0926 PST 30 September 1994. The location of the two deployments is shown in Fig. 2 of Lu and Lueck (1999) and is labeled TAMI1 and TAMI2. The instrument was nominally at 15 mab (meters above bottom). Cordova Channel is a minor side channel connecting the Georgia Strait basin to the Pacific Ocean. The channel is 30 m deep, 5 km long, and about 500 m wide at the 20-m isobath. The bottom is composed of fine gravel and slopes downward at less than 0.01 both to the north and south of the instrument. The elevation of the surface

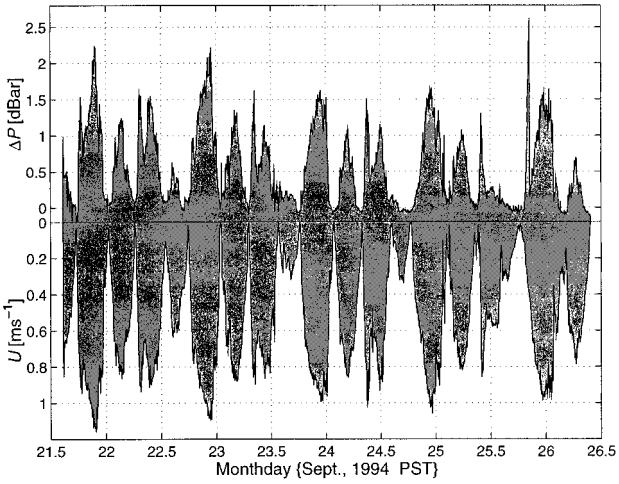

FIG. 3. Flow speed (lower panel) and the vertical displacement of the instrument deduced from the pressure difference between the tide gauges and the instrument (upper panel).

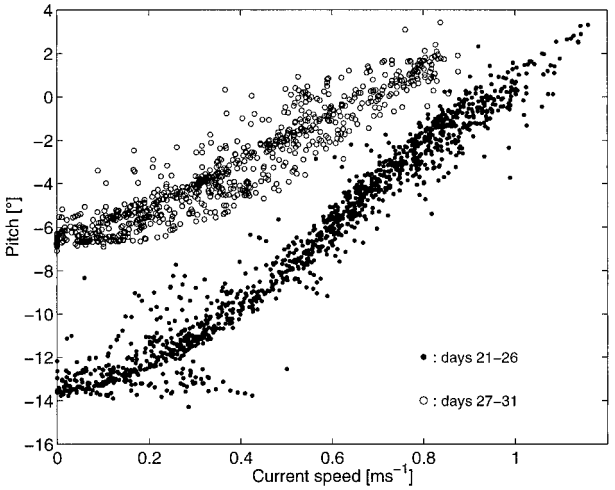

FIG. 4. Mean pitch angle vs speed from every 5-min sampling cycle. Open circles (lower curve) represent the first deployment, and closed circles (upper curve) represent the second deployment

varies by 1.5 m (peak to trough) and 90% of the variance of the current is explained by the M_2, K_1, S_2, and O_1 tidal constituents (Lueck and Lu 1998).

3. Time series

a. Low-frequency body motion

The time series of current measured by the instrument during the first deployment (Fig. 2) indicates that the orientation of the instrument is nearly always stable and directed along the axis of the channel. The orientation is expressed as cycles, that is, the heading divided by 2π rad. There are rapid changes of orientation only during the reversal of the tide and, for these brief intervals, the instrument may have a large angle of attack with respect to the current. The measured current speed and direction agree closely with the record from an ADCP located 90 m to the south of the moored instrument.

The low-frequency vertical motion of the instrument is derived by subtracting the average readings of two nearby tide gauges from the pressure measured by TAMI (Fig. 3). If the instrument maintains a constant elevation with respect to the bottom, this pressure difference will be constant. A constant value is subtracted to bring the pressure difference to zero during slack tide. The vertical position of the instrument is tightly correlated with current speed. The instrument moves down almost 2 m in a current of 1 m s^{-1} from its nominal depth during no flow, that is, the pressure difference increases by 2 db. The downward motion results from the deflection of the mooring line attached to the bottom of the mast, and the amount of deflection is consistent with the ratio of drag to buoyancy. A drag of 350 N is observed when the instrument is towed at the surface, and at a speed of 2 kt. An anomalously large vertical displacement occurred on day 25.8 with no corresponding extrema of speed. This event occurred shortly after the turning of the tide and was accompanied by a large roll, which suggests that the instrument was momentarily broadside to the flow.

The pitch of the instrument also changes in response to variations of current speed (Fig. 4). Ballast trimming for the first deployment (month days 21–26) produced a pitch of $-13°$ (nose down) at no flow, while an adjustment for the second deployment (months days 27–31) reduced the pitch to $-6°$ for zero flow. Ideally, the instrument should be fixed at a point directly above its anchor. However, its quasi-steady position and orientation are determined by the conditions of zero total force and torque. Without a current, there are three forces—weight (W), buoyancy (B), and tension (T)—all directed vertically (Fig. 5a). The instrument pitches downward because the center of weight is slightly forward from the center of buoyancy. As the current builds, drag forces the instrument backward, the cable draws it down and a negative lift (F_L) develops at the tail fins (Fig. 5b). The lift and drag both produce a counterclockwise torque around the bottom of the mast, which lifts the nose and reduces the downward pitch. With further increases in speed, the pitch reaches zero, and the lift at the fins becomes positive because of the downward bend of the rear portion of the horizontal fins (Fig. 5c). The bend is intended to counteract the increasing torque produced by increasing flow drag, but the lift is too small to compensate the drag. Therefore, the pitch continues to increase (although less slowly) with increasing flow speed (Fig. 5d). A decrease in the rate of change of pitch with speed is evident for pitch angles larger than $-2°$ (Fig. 4). The maximum pitch is 3° for both deployments. The pitch is between $-6°$ and 3° for 70% of the first deployment and between $-6°$ and 2° for 80% of the second deployment.

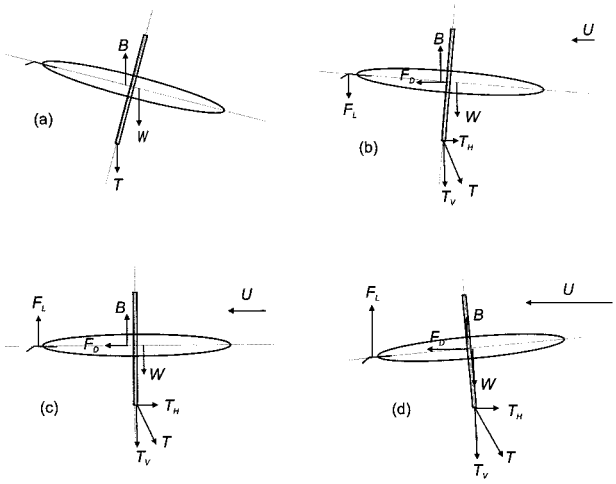

FIG. 5. Pitch and body forces on the instrument for flow speeds increasing from (a) zero to (d) to high speed. The forces are buoyancy (B), weight (W), drag (F_D), lift on the rear stabilizer (F_L), and cable tension (T), with subscripts H and V denoting the horizontal and vertical components, respectively.

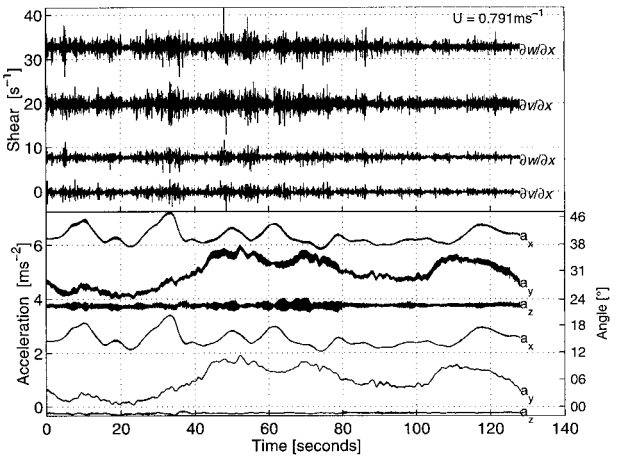

FIG. 6. A sample of unprocessed data of shear (upper panel) and accelerometer signals (lower panel) taken during a flow of 0.79 m s^{-1}. The upper traces in each panel are presented at full bandwidth, while the lower traces are low-pass filtered at 16 Hz. The curves have been offset for clarity. The filtered pitch and roll are offset by 18° and 7°, respectively. The rates of dissipation estimated with the vertical and athwartships probes are 1.56 and 1.52 × 10^{-5} W kg^{-1}, respectively.

b. Shear probes and accelerations

A sample of the unprocessed signals from the shear probes taken in a current of 0.79 m s^{-1} is shown in the upper panel of Fig. 6. This sample is 128 s long and represents a 100-m ''profile.'' The instrument samples the time derivative of the shear probe signals, which is converted to the along-flow gradients of velocity ($\partial w/\partial x$ and $\partial v/\partial x$) using the mean speed for this record. The upper pair of traces are the full bandwidth (43 Hz) signals and they show large and intermittent fluctuations typically seen in microstructure records. This characteristic is not significantly changed by low-pass filtering the data at 16 Hz (20 cpm) (lower pair of traces in the upper panel of Fig. 6). The choice of 16 Hz will be justified later. Vibrations and variations of pitch and roll are revealed by the accelerometer records in the lower panel of Fig. 6. Again, the upper three traces are presented at full bandwidth, while the lower three are low-pass filtered at 16 Hz. The signals from the longitudinal (a_x) and athwartships (a_y) accelerometers can be interpreted as pitch and roll, respectively, at low frequencies for which a scale is provided on the right-hand side. For frequencies below 1 Hz, the accelerometers report significant roll (5° peak) and pitch (4° peak). The measurements in Cordova Channel provided 30 records of unprocessed data, and the pitching and rolling shown in Fig. 6 are the second largest to be found in these records. The instrument does not sit as steadily in a current of 0.79 m s^{-1} as it did for L97 in currents weaker than 0.15 m s^{-1}. L97 reported peak pitch and roll fluctuations of less than 0.1°.

The vertical (a_z) and athwartships accelerometers show strong vibrations above 16 Hz, but below this frequency, there does not appear to be any correlation between the signals from the shear probes and the accelerometers. The accelerations, bandpass filtered between 1 and 16 Hz (not shown), are typically 0.03 m s^{-2}, or about 0.04 s^{-1}, when divided by the current speed, and nearly two factors of 10 smaller than the shear probe signals. An examination of all (30) other records of unprocessed data for speeds ranging from 0.3 to 1.2 m s^{-1} indicates that the accelerations scaled by speed are always small compared to the shear probe signals.

4. Spectra

The spectrum of the athwartship acceleration in a flow of 0.79 m s^{-1} (Fig. 7, thin line) indicates strong vibration at 17 and 34 Hz. Vibrations at 17 Hz are common at speeds above 0.5 m s^{-1}. Amplitudes vary by a factor of 10 and there are times when no significant vibrations occurred at any frequency. Figure 7 is an example of rather strong vibration. The frequency of vibration can vary by up to 2 Hz and does not scale with flow speed. One possible source for the vibrational energy is eddy shedding from the mooring cable, which has a diameter of $D = 0.0080$ m and a shedding frequency of $f = 0.2UD^{-1} = 20$ Hz. Our towed vehicle, which is mechanically similar to the moored instrument, also had a vibration near 18 Hz. Stiffening the mast of the towed vehicle, by welding thick-wall aluminum tubing into its interior, reduced the amplitude of vibrations 30 fold and shifted the vibration to 70 Hz. The simplest explanation for the vibration is that the mast is resonant near 18 Hz and that it vibrates in sympathy with energy in a neighborhood around this frequency and, thus, the frequency does not scale with speed. The spectrum of acceleration rises very steeply with decreasing frequency below 1

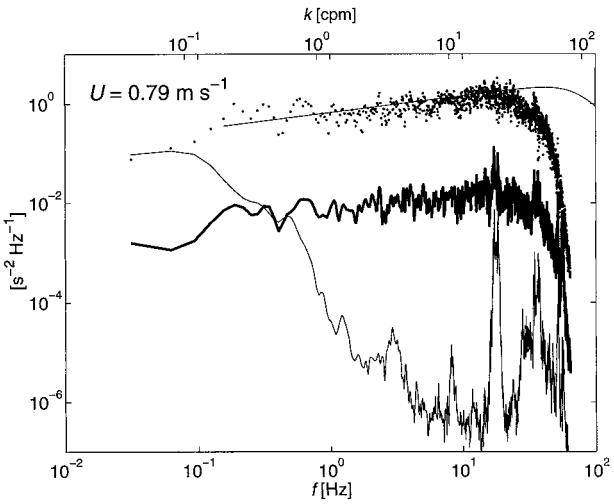

FIG. 7. Spectra of the time series shown in Fig. 7. Thin line—athwartship acceleration divided by speed, a_y/U; thick curve—shear, $\partial v_1/\partial x$; dots—average spectrum of $\partial v_1/\partial x$ and $\partial v_2/\partial x$ scaled by $[1 - \gamma^2(f)]$, where $\gamma^2(f)$ is the squared coherency between shear and acceleration; thin upper curve—Nasmyth spectrum for $\varepsilon = 1.5 \times 10^{-5}$ W kg^{-1}.

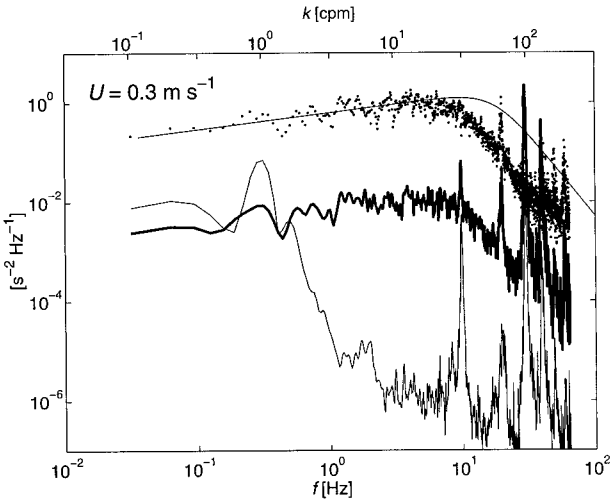

FIG. 8. Same as in Fig. 7 but for a current of 0.3 m s^{-1} and for $\varepsilon = 2 \times 10^{-6}$ W kg^{-1}.

Hz and this reflects the large contribution of roll to the measured signal. The athwartships accelerometer reports $g \sin(\phi)$, where g is the acceleration of gravity and ϕ the roll angle. Without rotation sensors, it is not possible to separate the roll and inertial signals. The spectrum of vertical vibration (not shown) is similar to that of athwartship vibrations above 1 Hz.

The spectrum of $\partial v/\partial x$ (Fig. 7, thick line) has a ⅓ slope at frequencies below 18 Hz and several peaks that are coherent with athwartship acceleration. The spectrum rolls off at higher frequencies due to electronic filtering and probe response. The shear spectrum is free from spectral peaks when it is multiplied by $(1 - \gamma^2)$, where $\gamma^2(f)$ is the squared coherency between shear and acceleration, and it agrees with the Nasmyth spectrum for a dissipation rate of 1.5×10^{-5} W kg^{-1} (Fig. 7, dots and upper thin line, respectively). Vibrations near 10 Hz are common during flows slower than 0.5 m s^{-1} and these vibrations also do not scale with speed and vary by a few hertz in frequency and a factor of 10 in amplitude (Fig. 8, thin curve). At 0.3 m s^{-1}, the shear spectrum (Fig. 8, thick line) has a ⅓ slope. The spectral peaks are highly coherent and removable (Fig. 8, dots).

The spectra of shear are free from vibrational contamination below 20 cpm for all flow speeds from 0.15 to 1.2 m s^{-1}. The upper limit of the inertial subrange (⅓-slope region of the shear spectrum) is easily deduced from the empirical universal spectrum of Nasmyth (Oakey 1982) and equals $k_s/30$, where k_s is the Kolmogorov wavenumber. This limit equals 17 cpm at a rate of dissipation of 10^{-4} W kg^{-1}, which is a little larger than the largest value observed in Cordova Channel. Thus, the instrument resolves two decades of the inertial subrange.

The velocity spectra are derived from the shear spectra by dividing the latter by $(2\pi k)^2$, where $k = f/U$ is the wavenumber in cycles per meter in the streamwise direction, f is the frequency in hertz, and U is the speed in m s^{-1}. The spectra have been corrected for the spectral resolution of the shear probe (Ninnis 1984) and for the small variations of the gain of the analog differentiators (calibrated to an accuracy of 0.5% with a spectrum analyzer). In the inertial subrange, the spectrum of cross-stream velocity fluctuations is given by

$$\Phi(\hat{k}) = \frac{4}{3} K \varepsilon^{2/3} \hat{k}^{-5/3}, \tag{1}$$

where $\hat{k} = 2\pi k$, ε is the rate of dissipation of kinetic energy, and $K = 0.5$ is the Kolmogorov constant for the one-dimensional velocity spectrum in the inertial subrange (Monin and Yaglom 1975; Grant et al. 1962; Edson et al. 1991). Thus, the spectrum should have a $-5/3$ slope and a level that depends only on the rate of dissipation, and spectra that are scaled by $k^{5/3}$ should be flat. Individual spectra scaled by $k^{5/3}$ are flat for both strong (Fig. 9a) and weak (Fig. 9b) stratification. The turbulence intensity relative to stratification is characterized, after Gargett et al. (1984), by $I = R_B^{3/4}$, where $R_B = (\varepsilon/\nu N^2)$ is the buoyancy Reynolds number, ν is the kinematic viscosity of water, N is the buoyancy frequency, and I is then the ratio of viscous to buoyancy scales. The rate of dissipation is estimated by averaging the individual spectral values:

$$\varepsilon_i = \left(\frac{3\Phi(\hat{k}_i)\hat{k}^{5/3}}{4K} \right)^{3/2}, \tag{2}$$

where $\hat{k}$ are all discrete wavenumbers from the interval of a spectrum that is not contaminated by body motions. Thus, the rate of dissipation is based upon the mean level of the velocity spectrum and not just on a single

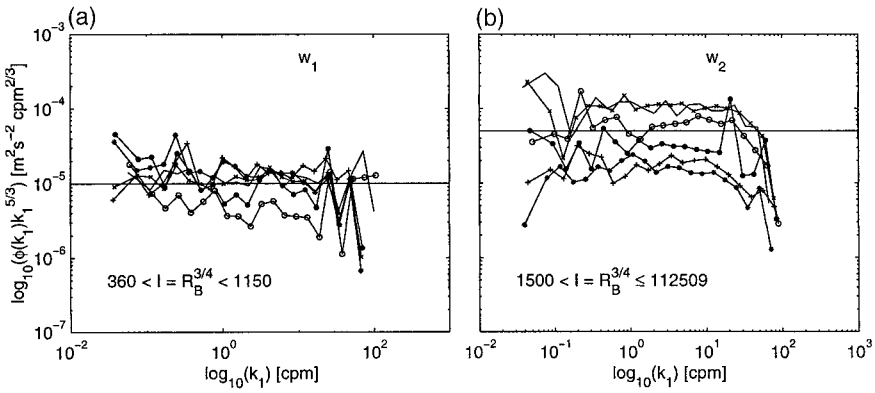

FIG. 9. Samples of vertical velocity spectra scaled by $k^{5/3}$ for (a) strong and (b) weak stratification.

spectral value. The inertial subrange technique produces consistent estimates of the rate of dissipation, and a regression of the six pairs of estimates, that can be drawn from four probes, shows a tight correlation over the range of 10^{-8}–10^{-4} W kg^{-1} (Fig. 10). Consistent estimates of the rate of dissipation are also obtained by the methods of spectral integration of the shear and the level of the inertial subrange with this instrument in a slow tidal channel at speeds from 0.03 to 0.15 m s^{-1} (L97).

The noise level of the dissipation estimates is difficult to estimate because the velocity ''contamination'' stems mainly from the turbulence; that is, vibrations, pitch,

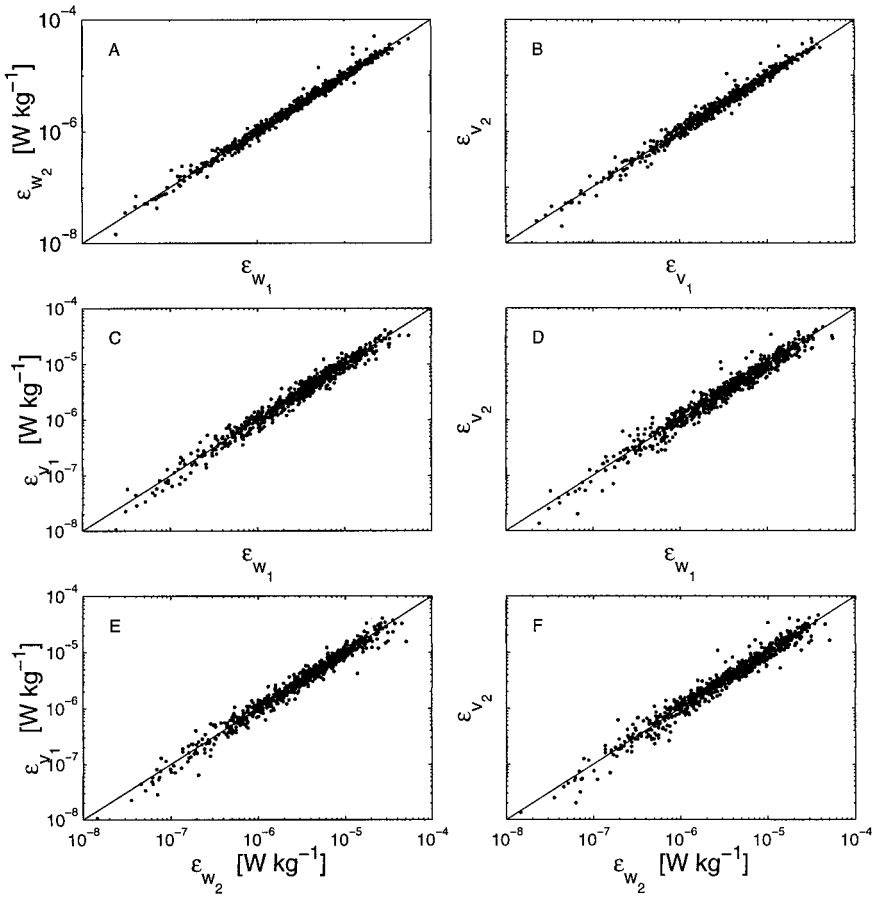

FIG. 10. Intercomparison of all dissipation rates measured by all probes. The estimates are consistent over a range of four decades.

and roll increase with turbulence intensity. Estimates never fell below 10^{-8} W kg^{-1}, but this may reflect conditions in the channel rather than the noise level of the instrument.

5. Discussion and conclusions

The large variations of pitch caused by changes of speed (Fig. 4) and the short-term fluctuations of pitch and roll (Fig. 6) are large compared to the motion of other horizontal profilers. Some of the ''excess'' motion is due to the intense turbulence in Cordova Channel, which is far greater than previous samples by horizontal profilers. However, it will not be difficult to reduce pitching motions. The torque produced by flow drag around the athwartship axis can be reduced nearly five fold by simply attaching the lower half of the mast with a hinge rather than a rigid mount. The moment arm will then be reduced from 1.5 to 0.35 m, which are the distances from the body center line to the bottom of the mast and hull, respectively. Similarly, the roll can be reduced by a double hinge (like the universal joint on a drive shaft). A fivefold reduction of pitch will result in variations of about 1°, which is commonly reported for towed vehicles (Fleury and Lueck 1994) and submarines (Osborn and Lueck 1985) and is quite acceptable for velocity measurements in the inertial subrange.

The very foundation of the technique presented here is the assumption that an inertial subrange actually exists. For unstratified turbulent flows, the inertial subrange exists for scales that are small compared to those of the energy and flux containing eddies, *and* large compared to the Kolmogrov scale. The small-scale limit is $30k_s^{-1}$, which equals 0.06 m at a rate of dissipation of 10^{-4} W kg^{-1} and is proportional to $\varepsilon^{-1/4}$. The large-scale limit can be no more than the distance to boundary or the scale of significant mean flow variations, whichever is smaller. This limit is 15 m for the data reported here. For stratified flow, the largest scales within the inertial subrange are set by the Ozmidov scale $(\varepsilon N^{-3})^{1/2}$. Dissipating eddies with scales larger than the Ozmidov scale are damped by gravity. The Ozmidov scale is never smaller than 1 m in Cordova Channel and rarely falls below 3 m. Thus, stratification did not limit the lower wavenumber for the inertial subrange technique. The lower limit is set by low-frequency body motions.

Although the use of the inertial subrange technique is fully justified for the data collected in Cordova Channel, such justification rarely existed for the data reported by L97, where the Ozmidov scale was seldom more than 0.2 m. Yet, they too found a well-defined $-5/3$ region indicative of an inertial subrange. Moreover, L97 used the shear variance to estimate the rate of dissipation and found excellent agreement between the observed spectrum of velocity and that predicted by (1). Thus, a velocity spectrum predicted for an inertial subrange appears to exist even when the conditions used for its prediction (Kolmogorov 1941) are not present. The inertial-subrange technique may have broader application than previously thought.

Acknowledgments. We gratefully acknowledge the major contributions made by Don Newman to the instrumentation of the moored instrument and by John Box to its mechanical aspects. Al Adrian provided logistics support during the measurements. The idea of a moored instrument sprouted from discussions with T. Osborn many years ago. This work was supported by the Office of Naval Research under Grant N00014-93-1-0362.

REFERENCES

Edson, J. B., C. W. Fairall, P. G. Mestayer, and S. E. Larson, 1991: A study of the inertial-dissipation method for computing air–sea fluxes. *J. Geophys. Res.,* **96,** 10 689–10 711.

Fleury, M., and R. G. Lueck, 1994: Direct heat flux estimates using a towed vehicle. *J. Phys. Oceanogr.,* **24,** 801–818.

Gargett, A. E., T. R. Osborn, and P. W. Nasmyth, 1984: Local isotropy and the decay of turbulence in a stratified fluid. *J. Fluid Mech.,* **144,** 231–280.

Grant, H. L., R. W. Stewart, and A. Moilliet, 1962: Turbulence spectra from a tidal channel. *J. Fluid Mech.,* **12,** 241–263.

Kolmogrov, A. N., 1941: Local structure in incompressible fluids at very high Reynolds number. *Dokl. Akad. Nauk. SSSR,* **30,** 82–85.

Lu, Y., and R. G. Lueck, 1999: Using a broadband ADCP in a tidal channel. Part I: Mean flow and shear. *J. Atmos. Oceanic Technol.,* **16,** 1556–1567.

Lueck, R. G., and Y. Lu, 1998: The logarithmic layer in a tidal channel. *Contin. Shelf Res.,* **17,** 1785–1801.

——, D. Huang, D. Newman, and J. Box, 1997: Turbulence measurements with a moored instrument. *J Atmos. Oceanic Technol.,* **14,** 143–161.

McPhee, M., 1992: Turbulent heat flux in the upper ocean under sea ice. *J. Geophys. Res.,* **97,** 5365–5379.

Monin, A. S., and A. M. Yaglom, 1975: *Statistical Fluid Mechanics.* The MIT Press, 874 pp.

Ninnis, R., 1984: The spatial transfer function of the airfoil shear probe. Ph.D. thesis, University of British Columbia, 109 pp. [Available from University of British Columbia, Vancouver, BC V6T 1Z4, Canada.]

Oakey, N. S., 1982: Determination of the rate of dissipation of turbulent energy from simultaneous temperature and velocity shear microstructure measurements. *J. Phys. Oceanogr.,* **12,** 256–271.

Osborn, T. R., and R. G. Lueck, 1985: Turbulence measurements from a submarine. *J. Phys. Oceanogr.,* **15,** 1502–1520.